Acta Mechanica 150, 39–51 (2001)

ACTA MECHANICA

Aerodynamic interactions of two airfoils in unsteady motion

S. L. Lan and **M. Sun,** Beijing, P.R. China

(Received May 3, 2000)

Summary. Aerodynamic interactions of two airfoils in tandem configuration moving parallelly forward and down at large angle of attack after an initial acceleration from rest are studied, using the method of solving the Navier-Stokes equations in moving overset grids. In the early time of the motion, force coefficients on the fore- and hind-airfoils are almost the same and are both enhanced in comparison with that of the single airfoil. The mechanism for the enhancement is that each airfoil sees a faster incoming flow because of the 'blockage' effect caused by the presence of the other airfoil. After the early time, for the cases having only horizontal spacing, C_L on the fore-airfoil keeps to be larger than that of the single airfoil, and the smaller the spacing is, the larger the C_L is; C_L on the hind-airfoil rapidly decreases to a lower level because of the interaction between the starting vortex of the fore-airfoil and the dynamic stall vortex of the hind-airfoil, and this detrimental effect becomes more severe as the spacing becomes smaller. C_d behaves similarly. When the hind-airfoil is lower in vertical position than the fore-airfoil and their horizontal spacing is small (e.g. the vertical and horizontal spacings are $0.25c$), large enhancement of the forces on the fore-airfoil (e.g. $C_L = 3.0$) and a noticeable enhancement on the hind-airfoil (e.g. $C_L \approx 2.2$) can be obtained.

1 Introduction

The flight of dragonflies and damselflies, which have two pairs of interfering wings, is obviously superior to that of other larger insects. They are capable of fast take-off, long-time hovering and quick maneuvre. Scientists have always been fascinated by their flight.

Kinematics data such as the stroke amplitudes and inclinations of the stroke-plane, wing beat frequencies and phase-relations between the fore- and hingwings, etc., were measured by taking high-speed pictures of tethered dragonflies (e.g. by Alexander [1]) and dragonflies in free-flight (e.g. by Norberg [2] and Wakeling and Ellington [3]). Using these data in quasi-steady analyses, not including the interaction effect between the wings, it was found that the mean lift force required for flight were much greater than the quasi-steady values and therefore, unsteady wing motions and flow interactions between the fore- and hindwings must play a major role in the flight of dragonflies [2]–[4].

Force measurement on a tethered dragonfly was conducted by Somps and Luttges [5]. It was shown that a single large lift peak occurred for each cycle rather than the double peaks expected from the sum of the forces from two independent wing pairs. This further suggested that the force generation was dominated by the unsteady interactions between the wings. In order to understand the dragonfly aerodynamics, it is needed to study the nature of the flow interactions between the fore- and hindwings in unsteady motions.

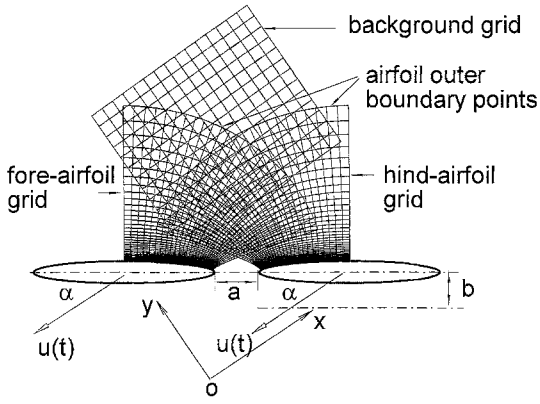

Fig. 1. A sketch of fore- and hind-airfoils and portions of the moving overset grids

In the present paper, we study the unsteady flow interactions between two airfoils that perform a simple but typical motion. In the motion, as sketched in Fig. 1, the two airfoils parallelly move forward and down with the same constant velocity and angle of attack after an initial start. This motion is representative of the downstroke motion of the wing sections for a dragonfly beating its wings in phase (parallel stroking). Dragonflies use parallel stroking for high-lift situations such as rapid accelerations, take-off and hovering [1] (In these modes of flight, forces used for weight support or acceleration are produced mainly by the downstroke [3]). Moreover, this motion is relatively simple. Therefore, it is chosen as the first step in our study of the unsteady flow interactions between the dragonfly fore- and hindwings. The method of numerically solving the Navier-Stokes equations using moving overset grids is employed in the study.

2 The computational method

The Navier-Stokes equations for incompressible flow are numerically solved using moving overset grids. For flow past a body in arbitrary motion, the govering equations can be cast in an inertial frame of reference using a general time-dependent coordinate transformation to account for the motion of the body.

A single-grid solver using the algorithm developed by Rogers et al. [7] was written by the present authors [6]. The algorithm is based on the method of artificial compressibility and uses a third-order flux-difference splitting technique for the convective terms and the second-order central difference for the viscous terms. Time accuracy in the numerical solutions is achieved by subiterating the equations in pseudotime for each physical time step. The single-grid solver is modified to overset grids for the present study.

With overset grids for the present study, as sketched in Fig. 1, each airfoil has a curvilinear grid, and they lie within a background Cartesian grid. Parts of the two airfoil grids overlap. The airfoil grids capture features such as boundary layers, separated vortices and vortex/airfoil interactions, etc. The background grid surrounds the airfoil grids and carries the solution to the far field. As a result of the oversetting of the grids, there is a hole region in each of the airfoil grids, as well as in the background grid. As the airfoil grids move, the holes and hole boundaries change with time. To determine hole-fringe points, the method known as domain connectivity functions by Meakin [8] is employed. Data are interpolated from one grid to another at the hole-fringe points and similarly at the outer-boundary points of the airfoil

grids. In the present study, there is no relative motion between the two airfoil grids but they move in the background grid.

For for field boundary conditions, at the inflow boundary, the velocity components are specified as freestream conditions while the pressure is extrapolated from the interior: at the outflow boundary, the pressure is set equal to the free-stream static pressure, and the velocity is extrapolated from the interior. On the airfoil surfaces, impermeable wall and no-slip boundary conditions were applied, and the pressure on the boundary is obtained through the normal component of the momentum equation.

The airfoil grids are generated by using a Poisson solver based on the work of Hilgenstock [9]. They are of O topology and extend approximately 0.9 chords from the airfoil surface. The background Cartesian grid has grid points concentrated at the airfoil's vicinity and extends to about 20 chords from the airfoil. Some portions of the grids are shown in Fig. 1.

3 Evaluation of solution accuracy

As with any numerical analysis, great care must be taken to insure the accuracy of the computed results. In the previous work of the present authors [6], the single-grid code was verified by the analytical solution of a flat plate, and validated by measured pressure distributions on a wing at $\alpha = 11.8°$. In order to verify the code for moving overset grids, flows around an airfoil were computed using both single-grid and the moving overset grids. The motion of the airfoil consists of three parts: the first translation, rotation and the second translation in the opposite direction from the first. The moving overset grids consist of two grids, i.e., an airfoil grid and a background grid. During the grid motion, the background grid remains stationary as the airfoil grid translates and rotates in it. Fig. 2 gives the comparison of the lift coefficient v.s. τ calculated by the single-grid and the moving overset grids. The large peaks in the lift coefficient are due to the fast acceleration, deceleration and rotation of the airfoil. Figure 3 compares the vorticity plots at one time instant ($\tau = 4.25$) from the two calculations. It is seen that results computed using the moving overset grids are in agreement with that of the single-grid.

Grid sensitivity was considered and will be discussed together with the calculated results in the next part of the paper.

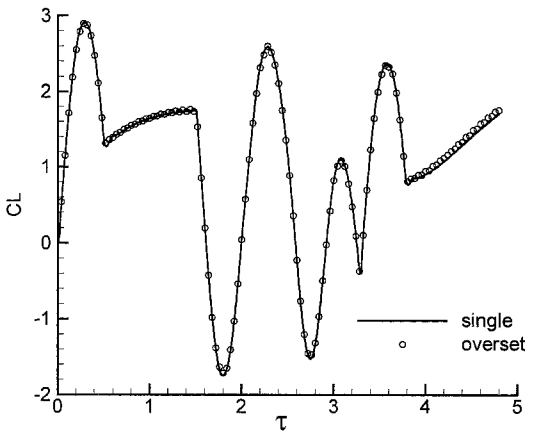

Fig. 2. Comparison between the lift coefficients of a moving airfoil calculated using a single grid and moving overset grids

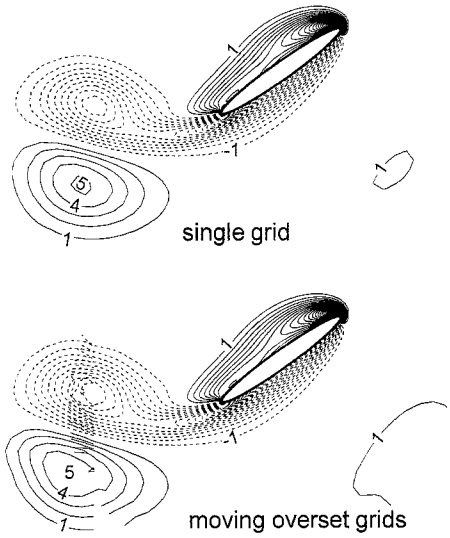

Fig. 3. Comparison between the vorticity contours of a moving airfoil at $\tau = 4.25$ calculated using a single grid and moving overset grids

4 Results and discussion

The airfoils are ellipses of 12 percent thickness. As can be seen in Fig. 1, a and b denote respectively the horizontal and vertical spacing, nondimensionalized by c (c denotes the airfoil chord length), between fore- and hind-airfoils. The two airfoils move forward and down parallelly with constant speed U after initial start. The speed of the airfoils during the acceleration is given as

$$u = 0.5U\left(1 - \cos\left(\frac{\pi t}{\tau_a}\right)\right), \qquad 0 \leq \tau \leq \tau_a, \tag{1}$$

where τ is the nondimensional time, defined as $\tau = tU/c$, τ_a the time at which the acceleration finishes. τ_a is set as 1.0 in the present study. The angle of attack of the airfoils α is set to 35°. The Reynolds number, Re, defined as $\mathrm{Re} = cU/v$ (v is the kinematic viscosity), is set to 1000. The above values of α and Re are typical ones employed in dragonfly flight. The horizontal distance between the fore- and hindwings of a dragonfly is about zero at the wing root and about 0.5c at the wing-tip. Therefore, in this study, we considered three values of a, $a = 0.05$, 0.25 and 0.5. The coefficients of lift, drag and moment (taken with respect to 0.25 chord location) are denoted by C_L, C_d and C_m respectively. As can be seen in Fig. 1, both C_L and C_d contribute to the vertical force which lifts the insect, and the sum of their horizontal components may provide a propulsive force. In order to reveal the interaction effect between the two airfoils, flows for a single airfoil of the same geometry and in the same motion are also calculated.

$a = 0.25$ and $b = 0$ (case A)

The present case of $a = 0.25$ and $b = 0$ is called case A for convenience in the later discussions. Figure 4 gives force and moment coefficients for the fore- and hind-airfoils (henceforth called FA and HA, respectively) and for the single airfoil (henceforth called SA). In the figure, results for two sets of overset grids are included. In the first set, each of the airfoil grids is

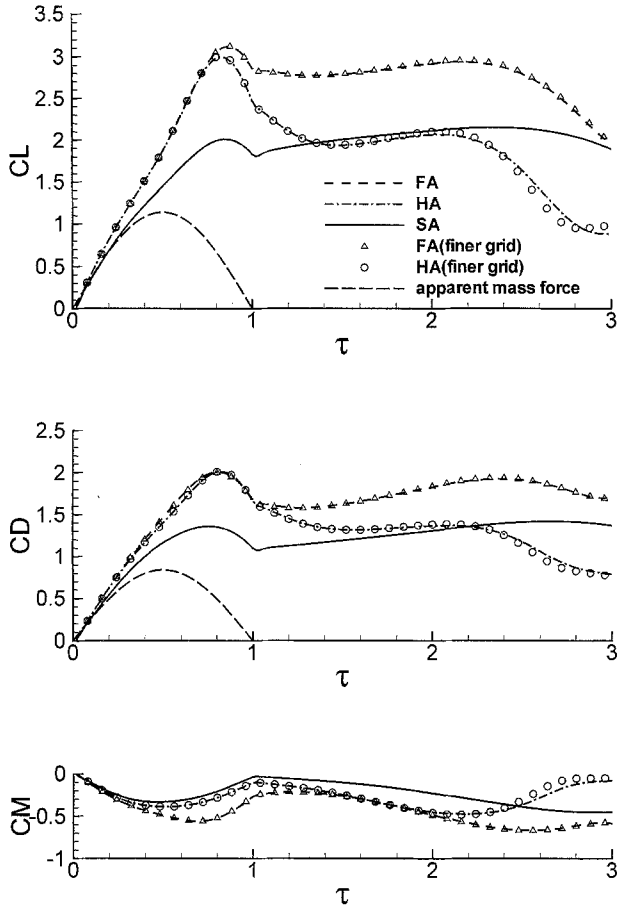

Fig. 4. Force and moment coefficients v.s. τ, $a = 0.25$. $b = 0$

52×153 (in normal direction and around the airfoil), and the background Cartesian grid is 117×103. In the other set, which is finer, the airfoil grids are 116×301, and the background Cartesian grid is 160×135. It is seen that there is almost no difference between the results of the two sets of overset grids. Therefore, for all the calculations for the two airfoils, the first set of overset grids is used.

It should be mentioned that dragonflies have small stroke angles (about 60°), and a typical section of the wing travels about $2.5 \sim 3.5$ chord lengths. Therefore, the calculations are carried out up to $\tau = 3$.

First, let's look at the results of SA. After the airfoil starts to move, its C_L increases rapidly and reaches its peak near the end of the acceleration, then it decreases slightly. In the constant-speed phase of the motion ($\tau \geq 1$), C_L maintains a large value of about 2 up to $\tau \approx 3$, and around this time, C_L starts to decrease due to the shedding of dynamic stall vortex as will be seen in a later part of the paper. C_d and C_m behave similarly. At the beginning of the motion, the forces on the airfoils should be mainly due to the acceleration of the apparent mass. For the single elliptical airfoil, the apparent mass forces are calculated analytically and included in Fig. 4. It is seen that between $\tau = 0$ and $\tau \approx 0.4$, C_L and C_d on SA are mainly from the apparent force.

Next we compare the results of FA and HA with that of SA. From Fig. 4, it is seen that in the early time of the motion ($\tau = 0$ to $\tau \approx 0.9$), C_L on the two airfoils are identical, and they are larger than of SA due to the mutual interaction of the two airfoils. After $\tau \approx 0.9$, C_L on

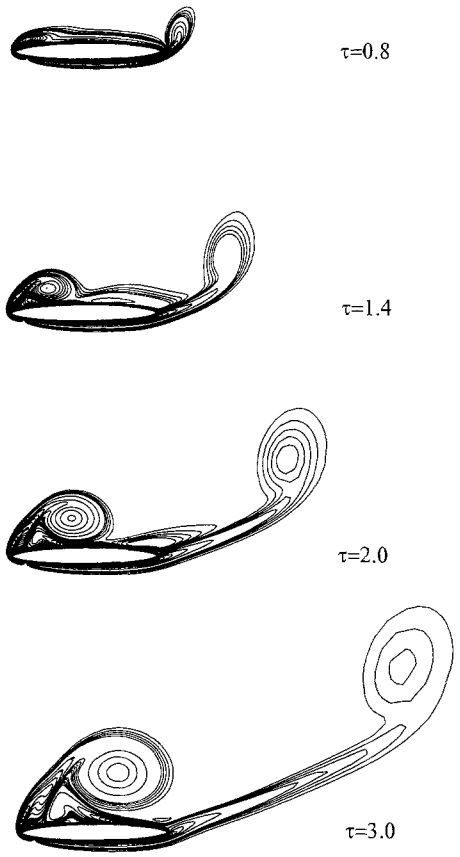

Fig. 5. Vorticity plots at various times, single airfoil

FA varies with τ in the same trend as that of SA, but its value is much larger (close to 3); C_L on HA decreases quickly (between $\tau \approx 0.9 \sim 1.2$) to the level of that of SA. C_L on FA stalls about the same time as that of SA, but C_L on HA stalls earlier. The C_d 's behave similarly.

In order to gain more insights in the nature of the flow interaction, vorticity, streamline plots and surface pressure distributions are given in the following. Figure 5 gives the vorticity plots at various times for SA. At $\tau \approx 3$, the dynamic stall vortex is shedding, resulting in the C_L stall shown in Fig. 4. Figure 6 gives the vorticity plots for FA and HA at the same time instants as that of SA. At $\tau = 0.8$ (and also at earlier times for which vorticity plots are not shown), the vorticity fields of FA and HA are almost the same, which is consistent with the fact that force coefficients on the two airfoils are identical in the early time of the motion. Comparing the vorticity plot at $\tau = 0.8$ with that of SA, it is seen that the positive and negative vorticity layers on the two airfoils are stronger, and the positive vorticity layers extend from the trailing edges further downstream than that of SA. This could give a larger total first moment of vorticity or fluid impulse, enhancing the forces on the two airfoils in the early time of the motion. The physical reason here is obvious. Because of the "blockage" effect caused by the presence of the other airfoil, each airfoil would see a faster incoming flow. As can be seen in the streamline plots in Fig. 7 at $\tau = 1$, the flow speed above the leading and trailing edge of FA or HA is larger than that of SA.

As time is increasing, the starting vortex of FA interacts with the dynamic stall vortex of HA (Fig. 6 at $\tau = 1.4$), making the dynamic vortex to become more diffused and to move downstream faster. This causes the force coefficients on HA to decrease sharply between

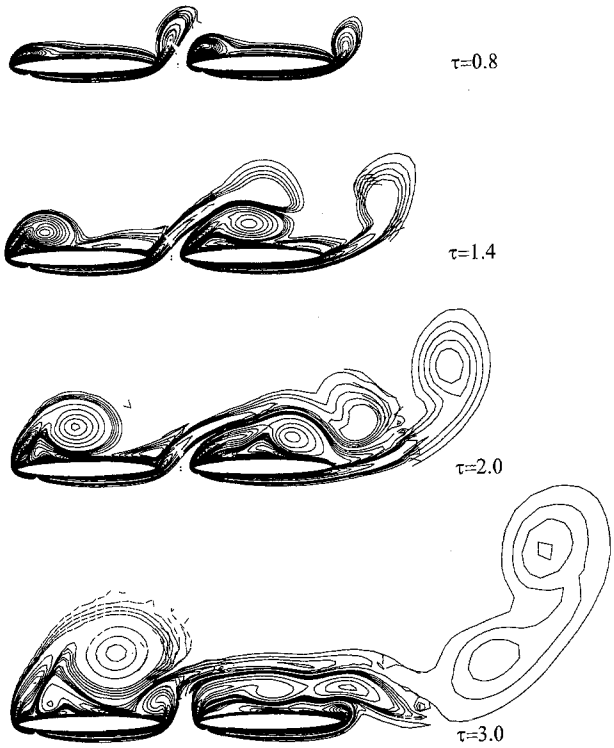

Fig. 6. Vorticity plots at various times, fore- and hind-airfoils, $a = 0.25$, $b = 0$

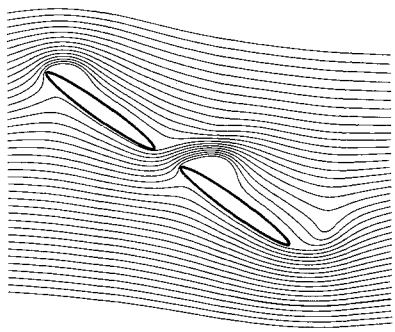

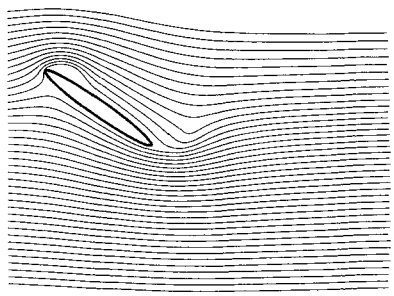

Fig. 7. Streamline plots at $\tau = 1.0$

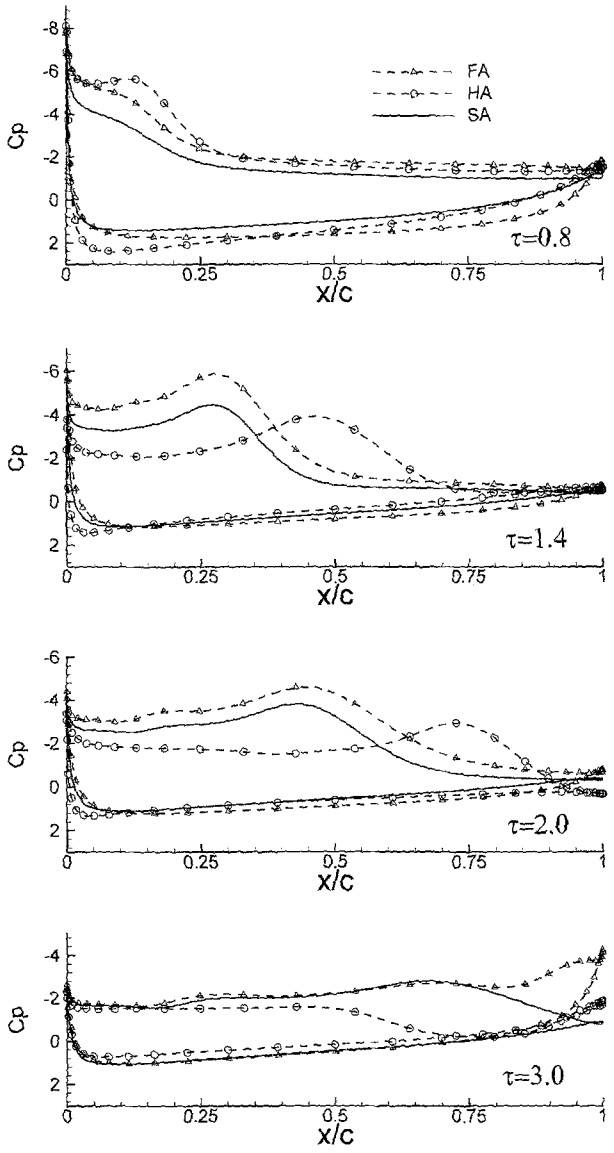

Fig. 8. Surface pressure distribution at various times

$\tau \approx 0.9 \sim 1.2$ and the airfoil to stall earlier. From the surface pressure distributions at various times, Fig. 8, the flow interaction effects are also seen clearly.

$a = 0.5$ and 0.05, $b = 0$.

As shown in Fig. 9, when the horizontal spacing between the two airfoils is increased to 0.5, compared with that of case A (Fig. 4), the enhancement of C_L due to the interaction becomes smaller. The drag coefficients behave similarly. The interaction between the starting vortex of FA and the dynamic stall vortex of HA, which is detrimental to the C_L of HA, is delayed to a later time, see Fig. 10.

When the two airfoils are very close to each other, $a = 0.05$, comparing the C_L in Fig. 11 with that of case A (Fig. 4), it is seen that the enhancement of C_L 's of both the airfoils in the early time of the motion and the enhancement of C_L of FA in later time become larger, but

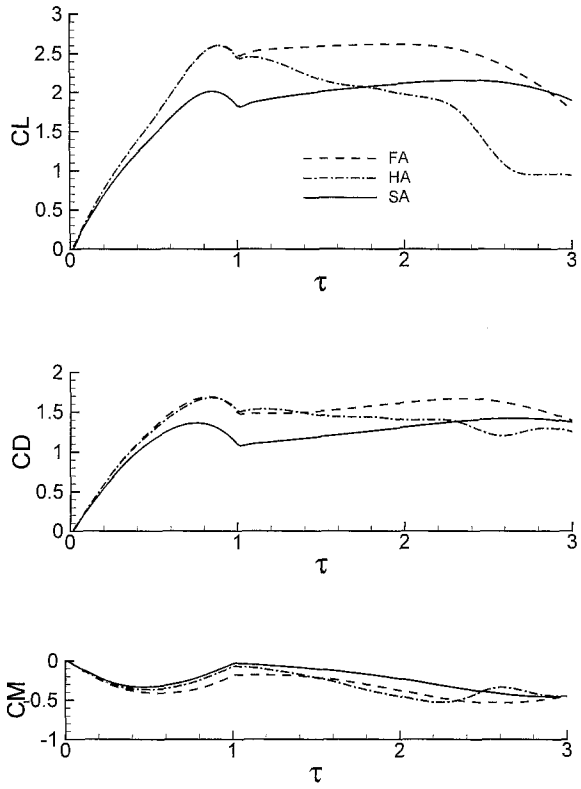

Fig. 9. Force and moment coefficients v.s. τ, $a = 0.5$, $b = 0$

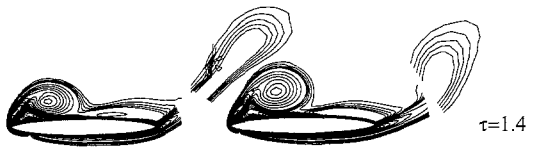

Fig. 10. Vorticity plots at $\tau = 1.4$, $a = 0.5$, $b = 0$

the interaction between the starting vortex of FA and the dynamic stall vortex of HA starts at a much earlier time and is more severe (Fig. 12), resulting in an earlier and larger decrease in C_L of HA. The drag coefficients behave similarly.

$a = 0.25, b = -0.25$ and 0.25.

For $a = 0.25$, $b = -0.25$, HA is higher in vertical position than FA and compared with that of case A, the distance between the two airfoils is larger. Figures 13 and 14 give the force and moment coefficients vs. τ and vorticity plots, respectively. In the early time of the motion, up to $\tau \approx 0.8$, similar to case A and other cases, C_L 's on FA and HA are almost the same and are enhanced by the interaction effect, but the enhancement is smaller due to the larger spacing. At later times, C_L on HA decreases for the same reason as in the previous cases, C_L on FA also decreases, which happens only in the present arrangement of the two airfoils. The drag coefficients behave similarly.

For $a = 0.25$, $b = 0.25$, HA is lower in vertical position than FA. The force and moment coefficients vs. τ and vorticity plots are given in Fig. 15 and Fig. 16, respectively. Although the spacing between the two airfoils is also larger than in case A, the enhancement of C_L on

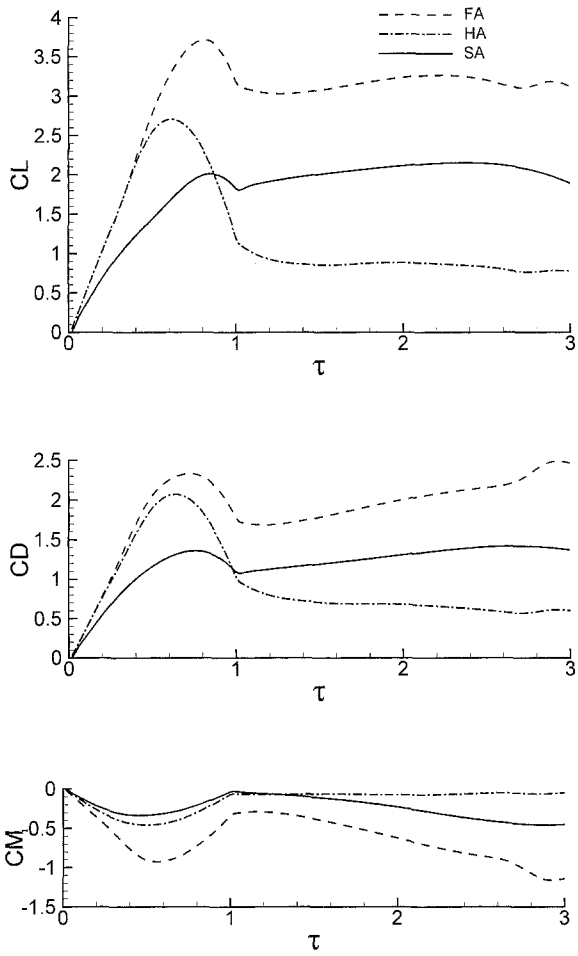

Fig. 11. Force and moment coefficients vs. τ, $a = 0.05$, $b = 0$

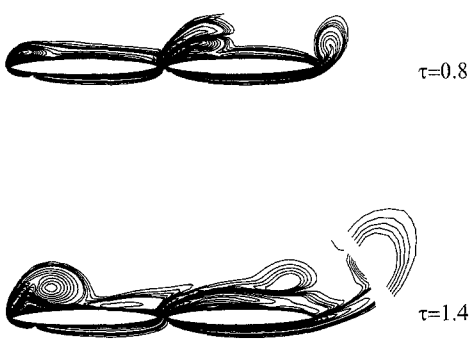

Fig. 12. Vorticity plots at various times, $a = 0.05$, $b = 0$

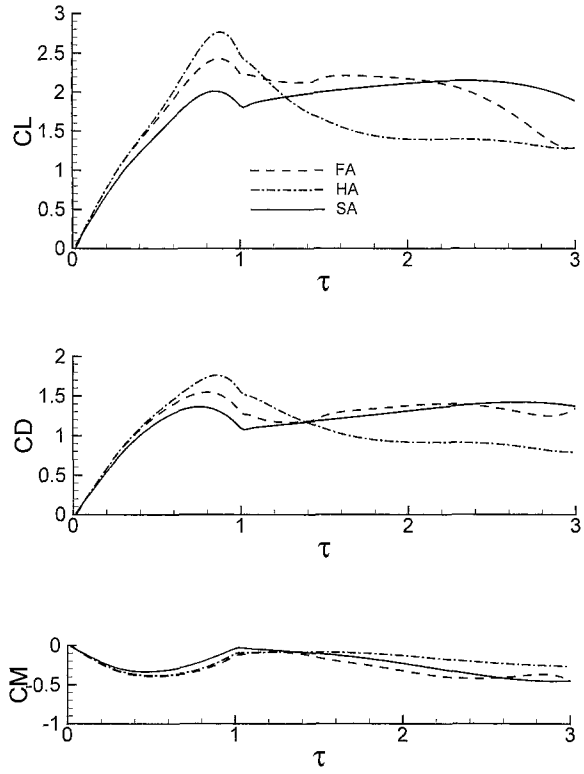

Fig. 13. Force and moment coefficients vs. τ, $a = 0.25$, $b = -0.25$

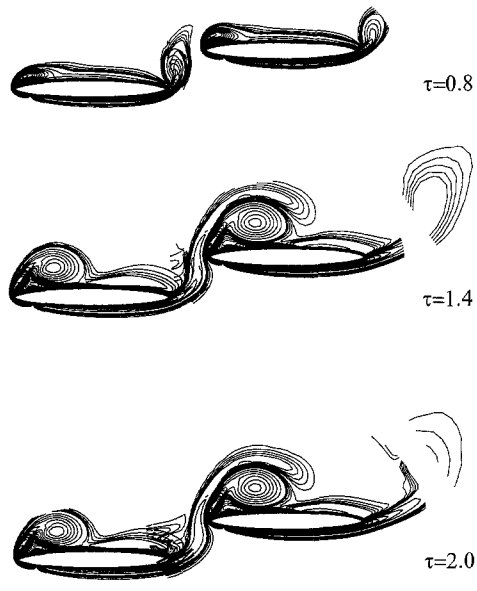

Fig. 14. Vorticity plots at various times, $a = 0.25$, $b = -0.25$

FA due to the interaction effect is larger than that of case A. The C_L on HA is also larger than of case A, since the starting vortex of FA is more distant from the dynamic stall vortex of HA than that in case A (as can be seen by comparing vorticity plots at $\tau = 1.4$ and 2.0 in Fig. 16 with that in Fig. 6), and the detrimental interaction of these two vortices is lessened.

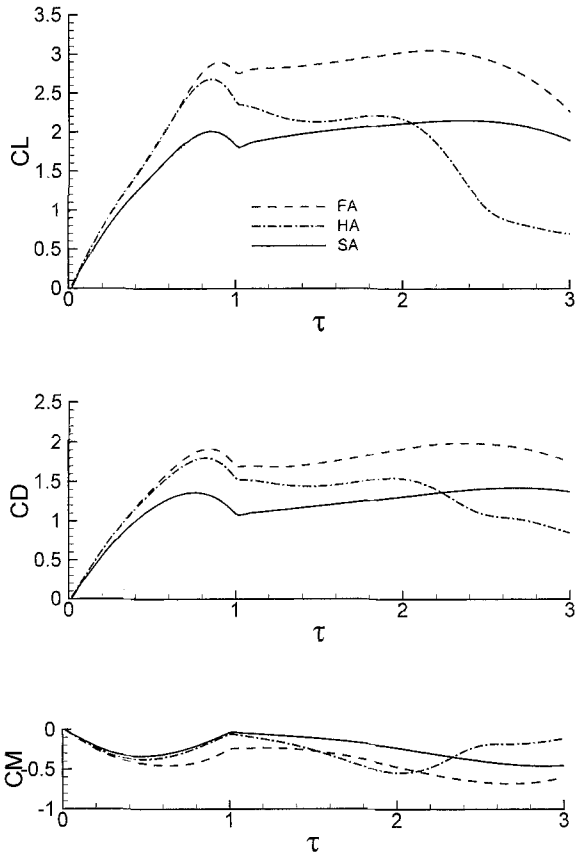

Fig. 15. Force and moment coefficients vs. τ, $a = 0.25$, $b = 0.25$

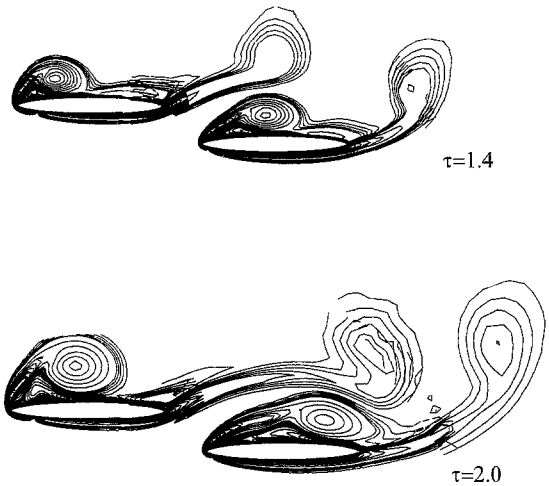

Fig. 16. Vorticity plots at various times, $a = 0.25$, $b = 0.25$

4 Conclusions

For two airfoils in tandem configurations moving parallelly forward and down at large angle of attack after an initial acceleration from rest, in the early time of the motion, force coefficients on the fore- and hind-airfoils are almost the same and are both enhanced in comparison with that of the single airfoil. The mechanism for the enhancement is that each airfoil sees a

faster incoming flow because of the "blockage" effect caused by the presence of the other airfoil. After the early time, for the cases having only horizontal spacing, C_L on the fore-airfoil keeps to be larger than that of the single airfoil, and the smaller the spacing is, the larger the C_L is; C_L on the hind-airfoil rapidly decreases to a lower level because of the interaction between the starting vortex of the fore-airfoil and the dynamic stall vortex of the hind-airfoil, and this detrimental effect becomes more severe as the spacing becomes smaller. C_d behaves similarly. When the hind-airfoil is lower in vertical position than the fore-airfoil and their horizontal spacing is small (e.g. the vertical and horizontal spacings are $0.25c$), large enhancement of the forces on the fore-airfoil (e.g. $C_L = 3.0$) and a noticeable enhancement on the hind-airfoil (e.g. $C_L \approx 2.2$) can be obtained.

Acknowledgements

This research was supported by National Natural Science Foundation of China, Grand No. 19725210.

References

[1] Alexander, D. E.: Unusual phase relationships between the forewings and hindwings in flying dragonflies. J. Exp. Biol. **109,** 379–383 (1984).

[2] Norberg, R. A.: Hovering flight of the dragonfly Aeschna juncea L., kinematics and aerodynamics. In: Swimming and flying in nature (Wu, T.Y., Brokaw, C. J., Brennen, C., eds.) pp. 763–781. New York: Plenum Press 1975.

[3] Wakeling, J. M., Ellington, C. P.; Dragonfly flight, II. Velocities, accelerations and kinematics of flapping flight. J. Exp. Biol. **200,** 557–582 (1997).

[4] Weis-Fogh, T.: Quick estimates of flight fitness in hovering animals, including novel mechanisms for lift production. J. Exp. Biol. **59,** 169–230 (1973).

[5] Somps, C., Luttges, M.: Dragonfly flight: novel uses of unsteady separation flows. Science **28,** 1326–1328 (1985).

[6] Lan, S. L., Sun, M.: Aerodynamic properties of a wing performing unsteady rotational motions at small Reynolds number. Acta Mech. (forthcoming).

[7] Rogers, S. E., Kwak, D., Kiris, C.: Numerical solution of the incompressible Navier-Strokes equations for steady-state and time-dependent problems. AIAA J. **29,** 603–610 (1991).

[8] Meakin, R.: Moving body overset grid methods for complete aircraft tiltrotor simulations. AIAA Paper 93–3350 (1993).

[9] Hilgenstock, A.: A fast method for the elliptic generation of three dimensional grids with full boundary control. In: Numerical grid generation in CFM '88, pp. 137–146 Pineridge Press 1988.

Authors' address: S. L. Lan and M. Sun. Institute of Fluid Mechanics, Beijing University of Aeronautics & Astronautics, Beijing 100083, P.R. China